Magma flow inferred from AMS fabrics in a layered mafic sill, Insizwa, South Africa

Eric C. Ferré, Cécile Bordarier and Julian S. Marsh

Department of Geology, Rhodes University, PO Box 94, Grahamstown 6140, South Africa

Abstract

The Insizwa sill, is a 25-km-diameter, >1000-m-thick layered mafic intrusion, part of the Karoo Igneous Province in South Africa. The peridotitic and gabbronoritic rocks are undeformed and mineral fabrics demonstrably result from magma flow. A horizontal, centimeter-scale model layering is visible in numerous outcrops. Plagioclase crystals are both tabular and elongated. Their preferred orientation, parallel to the layering, forms a foliation and a NW–SE lineation, respectively interpreted as the magma flow plane and flow direction. Throughout the 78 stations of this study (699 specimens), magnetic susceptibilities (K_m) range from 750 to 10,000×10^{-6} SI. The magnetic anisotropy (P_j) ranges from 1.03 to 1.08. Magnetic ellipsoids are both prolate and oblate (average $T_j \approx 0$). Anisotropy of magnetic susceptibility (AMS) fabrics are dominated by multidomain to pseudo-single domain magnetite. High-field magnetic experiments indicate that the paramagnetic contribution from the mafic silicates is less than 50% for low susceptibility rock types. The anisotropy results from magnetite grain shape solely as shown by no significant increase in P_j with increasing K_m. The magnetic lineation (305°, 05°) is consistent throughout the sill at various scales and coincides with the mineral lineation in average. In contrast, the magnetic foliation (125° NE 10°) is generally perpendicular to the mineral foliation and to the layering. Several explanations for this odd configuration are discussed. The variations of magnetic parameters across the layering and field observations point to a multiple injection. The magnetic lineation is consistent with the presence of a single feeder dike situated to the SE of the sill.

Keywords: sill; Mafic; AMS; layered; Insizwa; flow; igneous intrusion; igneous province; magma; magnetic anisotropy; magnetic susceptibility; tectonic setting; South Africa

1. Introduction

Our general understanding of magma flow in mafic dikes and mafic lava flows has greatly benefited from using the anisotropy of magnetic susceptibility (AMS) technique (Ellwood; Ernst; Ca and Glen). This technique can potentially yield the flow plane, the flow direction and even the flow sense (Knight and Walker, 1988).

Mafic horizontal sheet-like intrusions such as sills, laccoliths or lopoliths have so far received less attention from AMS studies. The mode of magma injection into single or composite sills is still poorly understood. This type of horizontal intrusion is common near the surface of the Earth (e.g., Meissner, 1985) but, due to the horizontal attitude, is generally not as prominent as dikes.

Mafic sills form an important volume component of the Karoo Continental Flood Basalt (CFB) province in Southern Africa. This Lower Jurassic CFB province displays exceptionally good exposures, along a several kilometer-thick section, from the top Drakensberg Formation basalt lava flows (Erlank and Cox) to the deeper doleritic and gabbronoritic sills and dikes intrusive into the underlying Karoo sedimentary sequence. The eroded remnants of the Mount Ayliff Complex occur as five thick, basin-shaped differentiated intrusions scattered over an area of about 3000 km^2. The Insizwa sill is one of these lobes and forms a >1000-m-thick sheet with an area of 520 km^2 (Lightfoot; Lightfoot and Cawthorn). Geophysical,

geochemical and petrological evidence support the successive injection of several distinct units (Cawthorn and Sander).

This study focuses on the source and the significance of AMS fabrics in the mafic sill of Insizwa. Our data are used to constrain the types of magma feeding and flow patterns. In theory, several feeding modes are possible either from a linear feeder such as a pipe (Fig. 1A) or from a planar feeder such as a dike or a fissure (Fig. 1B). Assuming that the sill grew by successive increments, several possible feeder geometries may result in distinct flow patterns, either parallel between successive intrusive sheets or cross-cutting (Fig. 1C). In this paper, we address the growth of a mafic sheet-like intrusion by discussing the homogeneity and consistency of magma flow at various scales from a few meters to that of tens of kilometers.

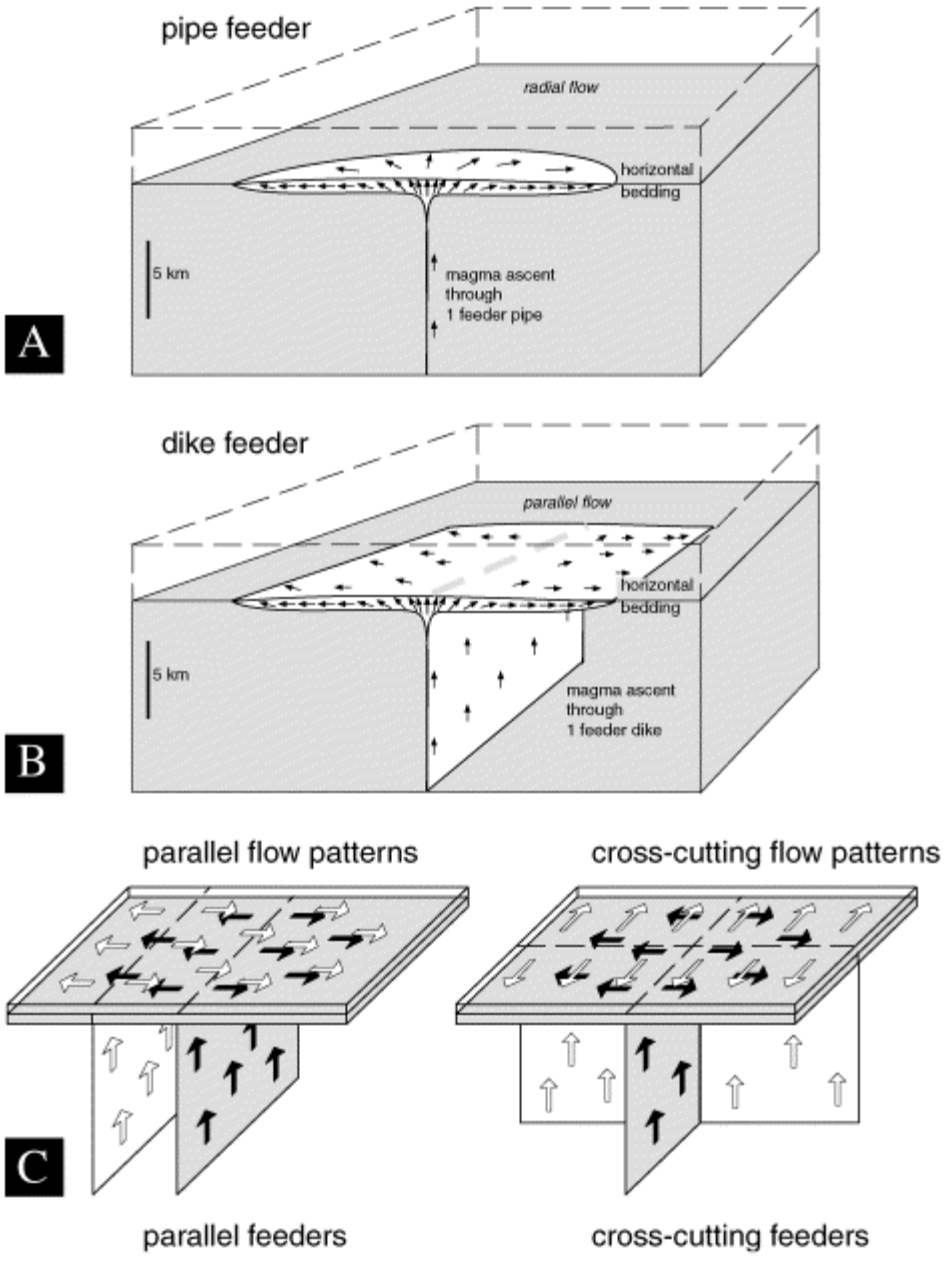

Fig. 1. Theoretical models of feeding systems for sheet intrusions. Magma flow lines shallow down away from the feeder. (A) Pipe feeder where magma supply originates from a single vertical pipe and resulting in magma radial flow away from the feeder. (B) Dike feeder where magma supply originates from a vertical dike and resulting in parallel flow. (C) Parallel dike feeders resulting in parallel flow lines, and perpendicular dike feeders resulting in cross-cutting flow lines.

2. Geological background

2.1. The Karoo setting

The intracratonic Karoo sedimentary sequence was deposited, from Permo-Carboniferous to early Jurassic, in a basin overlying the Archaean Kaapvaal Craton in the north and on the Proterozoic Namaqua–Natal Belt and Paleozoic Cape Supergroup in the south (Smith, 1990). The main sedimentary formations, of a total thickness ≤6 km, are named, from base to top: Dwyka, Ecca, Beaufort, Molteno, Elliot and Clarens. The Karoo igneous event, with the emplacement of the volcanic Drakensberg Group, marked the end of the Karoo basin evolution. This event consisted in the continental scale eruption of tholeiitic basalt lava and the intrusion of numerous dikes and sills of similar compositions at 183±1 Ma (Duncan et al., 1997 and references therein). Contemporaneous magmatism of the Ferrar Province in Antarctica and Australia has been correlated with the Karoo event and breakup of Gondwana (Encarnacion et al., 1996). The total volume of the Ferrar–Karoo province is estimated to $\approx 2.5 \times 10^6$ km^3 (Duncan et al., 1997).

The emplacement style of Karoo intrusions varies with stratigraphic height through the sedimentary sequence. At the base, thin sills dominate in the Dwyka and Ecca Groups. Sills and sheets reach their maximum development in thickness and abundance within the Beaufort Group and are frequently transgressive and basin-shaped (Chevallier and Woodford, 1999). Cross-cutting dikes are also present in the Beaufort Group but become more prominent in the overlying Molteno, Elliot and Clarens Formations, which form the upper part of the sedimentary sequence.

The tectonic setting of the Karoo igneous event can be constrained by the sedimentary environment of the last part of the Karoo cycle. Interpretations range from a subduction-related foreland basin (Catuneanu and Pysklywec) to continental rifting preceding Gondwana breakup (Turner, 1999). The Karoo province has a large volume of material erupted in a relatively short time eruption (Duncan et al., 1997) and usually this implies an origin through mantle plume activity (White and Campbell). In other mantle plume-related igneous provinces, magma flow direction is thought to be radial and circumferential with respect to the plume center (Ernst and Ernst). However, in the case of the Karoo, the site of plume(s) (Chevallier and Woodford, 1999) or whether a plume is involved at all (Hawkesworth et al., 1999) remains unresolved.

2.2. The Insizwa sill

The Insizwa sill (Fig. 2), is the largest of a number of transgressive sheet-like lobes intrusions forming the Mount Ayliff Complex, the others being Horseshoe, Ingeli, Tabankulu and Tonti. The total exposed thickness of the Insizwa sill, measured from a number of vertical boreholes is in excess of 1200 m and gravity data suggest substantial thickness variations (Sander and Cawthorn, 1996).

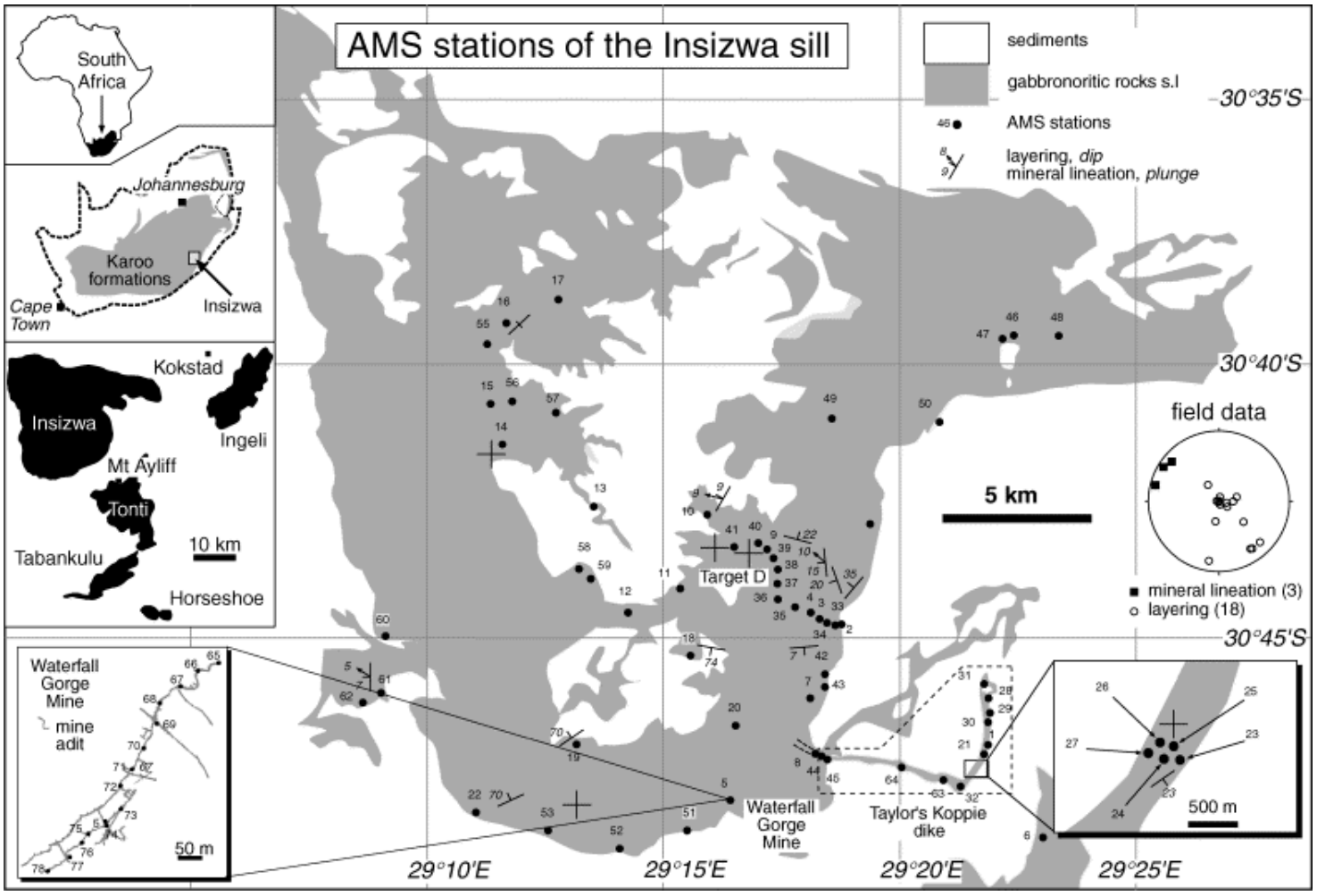

Fig. 2. Sampling and localization map of the Insizwa sill. Inset on the left shows the other lobes of the Mount Ayliff Complex. Shadowed insets display details of the sampling areas for Waterfall Gorge Mine and Taylor's Koppie Dike. Structural symbols represent features measured in the field where possible.

The intrusion consists of a thick, grossly layered sequence of mafic and ultramafic ortho-, meso-, and adcumulates. Olivine-rich lithologies, including a thick (up to 350 m in places) ubiquitous peridotite orthocumulate dominate towards the base and evolved quartz-bearing monzodiorites and granodiorites occur at the roof. In addition, small Ni–Cu–PGE massive sulfide deposits are hosted by the footwall hornfelses and basal gabbroic rocks (Maske and Cawthorn, 1986). The largest known deposit, visible along the footwall at Waterfall Gorge Mine (Fig. 2), consists of sulfide lenses and veins. Numerous dikes cut or branch to the sill (Fig. 3A) and some, such as Taylor's Koppie dike (Fig. 2), have been considered as possible feeders to the Insizwa sill.

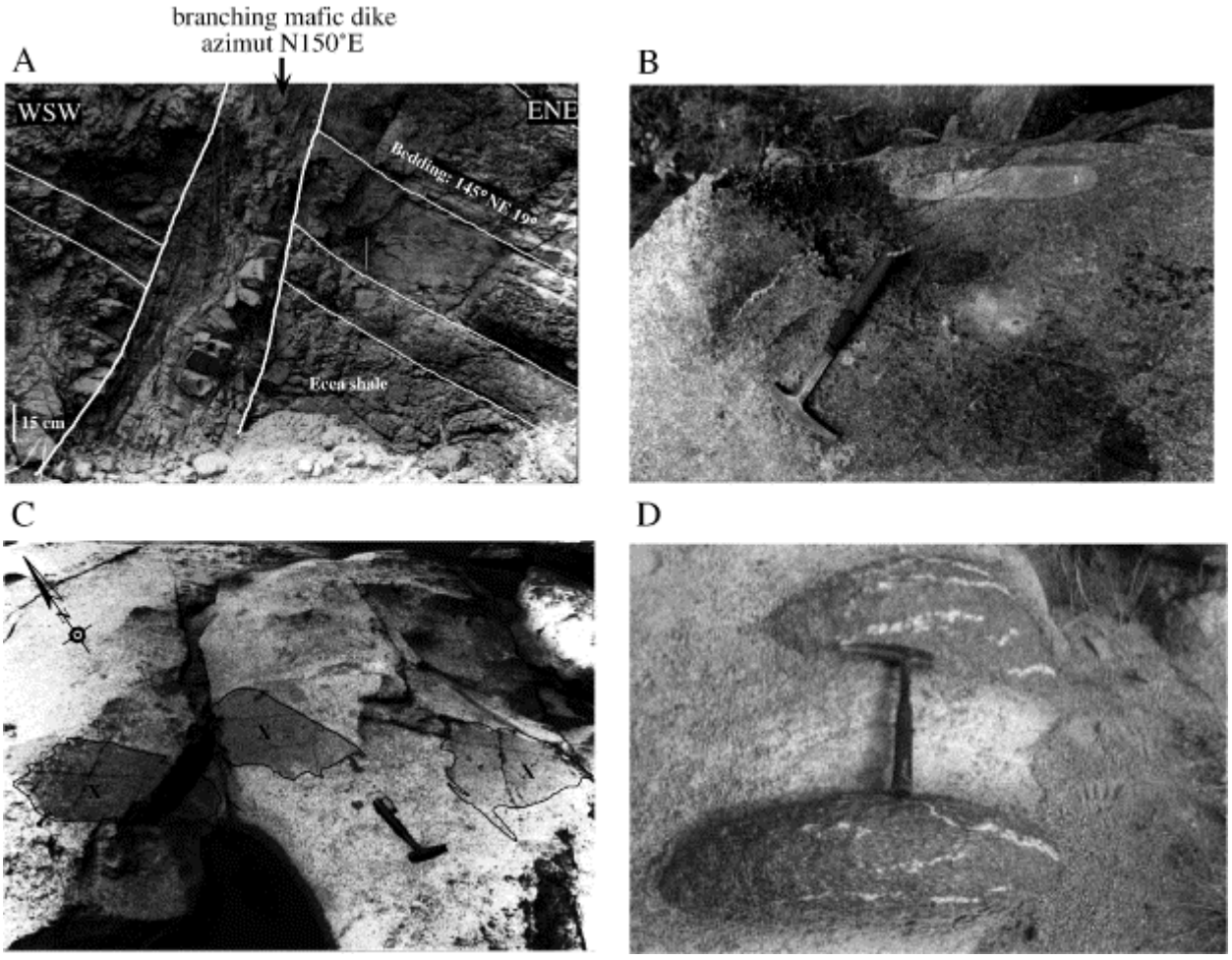

Fig. 3. Field photographs. (A) Minor branching mafic dike below the Insizwa sill. Note the perpendicular attitude with respect to the bedding suggesting post emplacement tilting. (B) Elongate xenoliths of anorthosite in gabbronorites along the Target area near station #008. (C) Angular and irregular xenoliths of gabbronorite (x) in a norite at station #009. (D) Plagioclase veinlets perpendicular to the horizontal layering and parallel to xenolith elongation in gabbronorites at station #16.

The Insizwa sill intruded in the Beaufort sandstones, close to the Ecca-Beaufort boundary, at a depth of about 2.5 km. The lherzolitic Horseshoe sill, situated 35 km to the SE of Insizwa and often interpreted as originally connected to the Insizwa sill (e.g., Sander and Cawthorn, 1996), intruded at a greater depth in the Ecca shales. The Insizwa sill is underlain by 2.5 km of Karoo strata which, in turn, are underlain by the Namaqua–Natal Proterozoic basement (De Decker, 1981). The sediments at the roof of the Insizwa sill rest horizontally and undeformed on granodioritic and monzonitic rocks. Below the sill, deformation of the Ecca shales is limited to kilometer-scale wavelength, upright, open folds and a few minor normal faults. The Beaufort sandstones are, at the outcrop scale, practically undeformed. The bedding of the sediments is often not visible in the contact aureole, but further away it is nearly parallel to the contact and even further away (>1 km), it becomes gradually horizontal.

Magmatic structures are visible in places in the gabbronorites and include a sporadic, weakly developed zones of centimeter-scale modal layering, oriented lenses and xenoliths of anorthosite (Fig. 3B), and aligned plagioclase crystals forming a mineral lineation. The layering was measured at 18 localities but the mineral lineation could be measured at three stations only (Fig. 2). The preferred orientation of platy plagioclase crystals is systematically parallel to the layering. Wherever it is visible, within the Insizwa sill at more than about 1 km distance from the margin, the compositional layering of the gabbronorites dips gently or is horizontal (Fig. 2). This is confirmed by data from more than 10 vertical boreholes cutting through the whole sequence (e.g., Sander and Cawthorn, 1996). The layering becomes gradually steeper near the margins (up to 70°) and dips typically towards the center of the sill (Fig. 2), which gives the sill a dish geometry.

Oriented thin sections (48×60 mm) have been cut in 14 representative blocks to investigate internal fabrics. Sample #066 (Fig. 4) is a plagioclase peridotite containing approximately 40% olivine, 40% pyroxene and 15% plagioclase (mode obtained by point counting). Sections were digitized at a high resolution (1442×1810 pixels) and images were processed using the Intercept software (Robin and Launeau). Plagioclase carries the highest degree of fabric anisotropy with a maximum at 7% (SR=shape RATIO=1.07). The average foliation calculated with this method strikes 21° and dips NW 47° (parallel to the compositional layering) and the lineation 203° 02°.

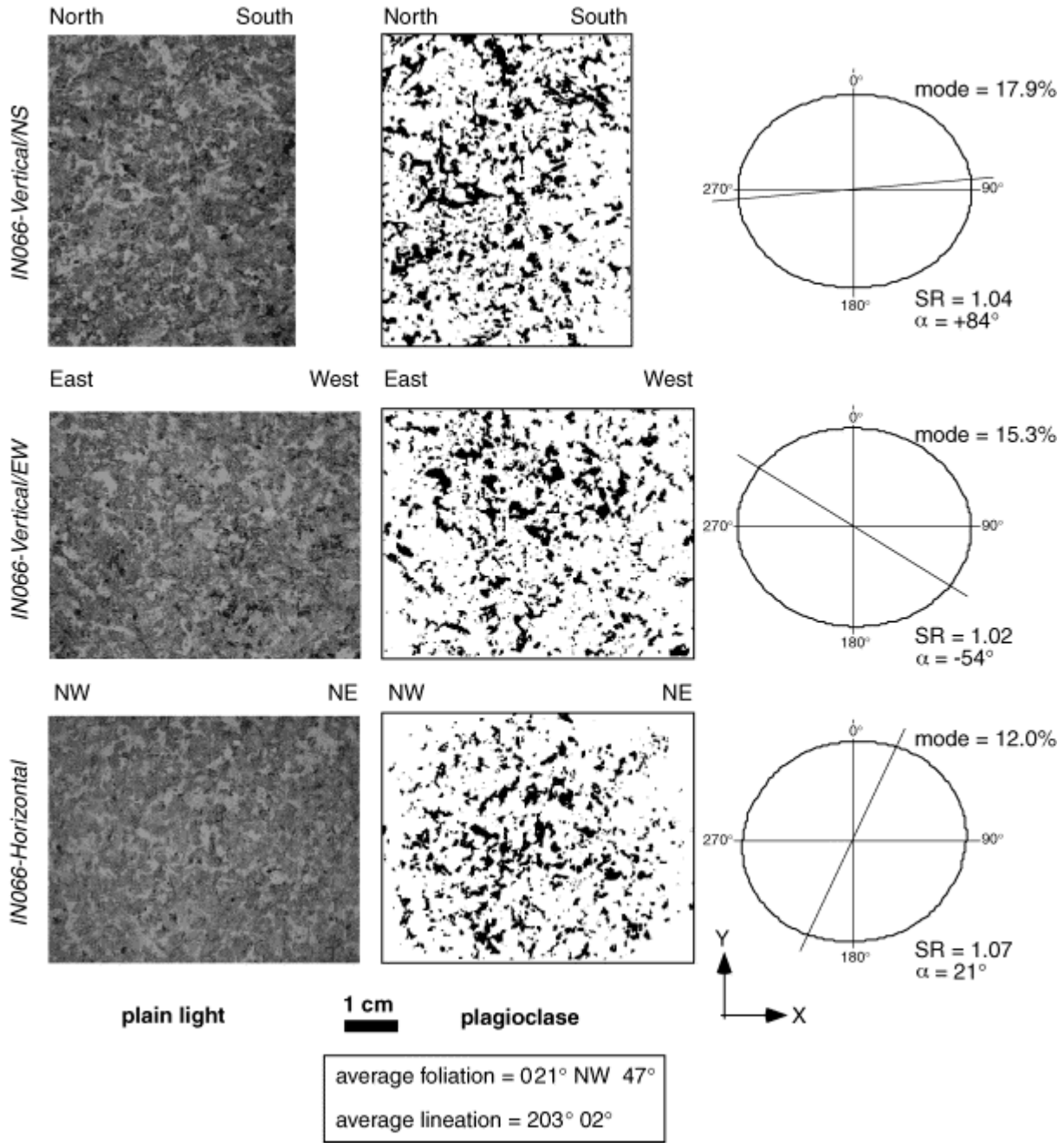

Fig. 4. Image analysis for sample #066 (Waterfall Gorge Mine, plagioclase peridotite). Three perpendicular sections were cut from a block along horizontal, a vertical NS and vertical EW planes. Images were digitized at high resolution and analyzed using the Intercept method (Launeau and Robin, 1996). SR: shape ratio measures the degree of fabric anisotropy along a section. α is the angle between the long axis of the shape preferred orientation ellipse and the *X*-axis of the thin section.

The Insizwa sill has been subdivided into several zones and units within the zones (Scholtz; Lightfoot and Cawthorn). The zone stratigraphy is consistent across the intrusion but that of units varies considerably and some units are missing or duplicated in some boreholes. The following description is an idealized stratigraphy with the Lower, Central and Upper Zones from base to top.

– The Lower Zone (LZ) is dominated by olivine-rich gabbronorites with a well demarcated plagioclase peridotite layer up to 350 m thick. The LZ is further subdivided into three units, chill phase, olivine-hypersthene gabbronorite and plagioclase peridotite. The footwall contact metamorphic aureole is thinner than 60 m. The contact between hornfels and igneous rocks is sharp. The *LZ fine-grained gabbro* (<10 m

thick) displays highly resorbed anhedral grains of cumulus olivine enclosed in a pyroxene-plagioclase groundmass with ≈2% of interstitial biotite. Pyroxenes form granular aggregates while plagioclase occurs as small radiating 1-mm-long laths. Accessories include quartz, K-feldspar, apatite and sulfide. The *LZ olivine-hypersthene gabbronorite* (<20 m thick) is fine-grained and consist of cumulus olivine and plagioclase in a matrix of bronzite and augite. Olivine gradually increases upward to become the major constituent in the LZ plagioclase peridotite unit. Biotite is interstitial and associated with Fe–Ti oxides. The *LZ plagioclase peridotite* shows equant-subequant cumulus olivine (35–80%) often with inclusions of euhedral chromite (≈5%), spinel, intercumulus poikilitic plagioclase (15–60%), orthopyroxene, augite (≤0.5 cm), interstitial biotite and minor ilmenite. Olivine percentage gradually increases upward in this unit too. The top contact of the LZ plagioclase peridotite is marked by the appearance of cumulus plagioclase.

– The Central Zone (CZ) is about 600 m thick and dominated by quartz-bearing and olivine-bearing gabbronoritic mesocumulates grading in places into olivine-rich layers. A few gabbroic layers contain minor amounts of K-feldspar, quartz and hornblende. The percentage of subhedral to euhedral chromite decreases upwards. The transition from LZ to CZ occurs over a few meters. At the top of the CZ, olivine disappears, pyroxene, plagioclase, hornblende, K-feldspar and quartz percentage increase up to 50% and anhedral, late-crystallized ilmenite becomes common and abundant.

– The Upper Zone (UZ) forms scattered outcrops along the upper contact (<110 m) and consists of granophyres and quartz–monzonites with cumulus plagioclase and intercumulus quartz, K-feldspar, hornblende and biotite. Pegmatite veins cut through the hornfels at the hanging wall.

Several lines of evidence suggest that the sill formed from the multiple intrusion of distinct magmas, e.g. distinct chromite chemical trends in different profiles of the Insizwa sill (e.g., Cawthorn et al., 1991) and xenoliths of one petrographic unit into another one (Fig. 3C; Sander, 1993). New geochemical data also support this hypothesis (Maier et al., accpted for publication).

Magmatically driven fluids have been recognized elsewhere in the Karoo (Duane and Brown). However, at Insizwa, the unaltered nature of the olivines suggests that such fluids have not percolated through the gabbronorites. A similar insulation from hydrothermal systems has been observed elsewhere and explained as the result of the inward-progressing magmatic crystallization front (Taylor, 1988).

A network of N110° striking vertical faults has been identified in the field and correlated on aerial photographs with 270 lineaments throughout the Insizwa area.

3. Magnetic susceptibility methodology

The samples were collected from 78 stations throughout the Insizwa sill (Fig. 2), at an average spacing of 3 km, precisely positioned with a GPS. Three oriented cores were collected at each station, at a distance of 1–2 m from one another. Cores were long enough to yield at least three specimens, giving at least nine specimens per station and 700 specimens in total (diameter=25 mm, LENGTH=22 mm). Cores were collected from massive rocks and away from faults and fractures.

Measurements were carried out at low alternating inductive field ($\pm 4.10^{-4}$ T, 920 Hz) on a Kappabridge KLY-2 susceptometer (Geofysika, Brno) in the *Laboratoire de Pétrophysique* in Toulouse, France. Values are reproducible over the 0.05×10^{-6} to 0.5 SI range of susceptibilities and down to 1.002 anisotropies. Each specimen was measured in 15 different positions to calculate the magnitude and orientation of the magnetic ellipsoid with an accuracy <5°. Thermomagnetic properties were determined in low field using a CS-2

furnace attached to the KLY-2. The hysteresis properties of five specimens were measured on a Vibrating Sample Magnetometer (Princeton Applied Research) at the IRM (Minneapolis, USA).

The principles of the anisotropy of magnetic susceptibility (review in Tarling and Hrouda, 1993) are given below. A rock sample modifies the intensity of the applied low magnetic field in which it is immersed. The ratio between the induced and the inducing magnetic fields is the magnetic susceptibility K. Spatial variations of K are given as a second rank tensor whose representation is an ellipsoid with $K_1 \geq K_2 \geq K_3$ as principal axes. K_1 is the magnetic lineation and K_3 is the pole to the magnetic foliation. The mean magnetic susceptibility K_m is the arithmetic mean of the principal axes [$K_m = 1/3(K_1+K_2+K_3)$]. The corrected degree of anisotropy is $P_j = \exp\sqrt{\{2[(\eta_1-\eta)^2+(\eta_2-\eta)^2+(\eta_3-\eta)^2]\}}$ with $\eta = (\eta_1+\eta_2+\eta_3)/3$, $\eta_1 = \log K_1$, $\eta_2 = \log K_2$ and $\eta_3 = \log K_3$ (Jelínek, 1981). Table 1.1 of Tarling and Hrouda (1993) has an erroneous expression of η. The shape of the ellipsoid is represented by the parameter T_j [$T_j = (2\eta_2-\eta_1-\eta_2)/(\eta_1-\eta_3)$] with oblate shapes for $0 \leq T_j \leq 1$ and prolate shapes for $-1 \leq T \leq 0$. The variation coefficient of K_m is cv_{Km} [$cv_{Km} = 100 \times \sigma_{Km}/K_m$, in %] where σ_{Km} is the standard deviation of K_m. αK_1 and αK_3, the larger half angle of the principal diameters of the 95% confidence ellipses about K_1 and K_3 of a single specimen represent the measurement error. Within-station variability of the orientation of the AMS principal axes are given by σK_i, which is the average angle between K_i of the specimens and the vectorial mean of the station specimens.

4. Magnetic susceptibility and AMS data

4.1. Magnetic susceptibility

The main magnetic features of the Insizwa rocks are listed in Table 1. Data for each station are given in Table 2. Within-core variations of magnetic susceptibilities are independent from the distance of the specimens from the outcrop surface. Hence, weathering-related variations are considered negligible compared to those resulting from the original rock composition. The within-core variation of K_m is <10% in 77% of cores (194 cores) and the within-station variation of K_m is <20% in 70% of stations (64 stations). Samples from mineralized areas, such as Waterfall Gorge or Taylor's Koppie dike (Fig. 2), display a larger variability.

Table 1. Stratigraphy, magnetic susceptibility and AMS of the Insizwa rocks

Zone	Unit	Code	Thickness[a] (m)	No. of specimens	$K_m \pm$ stdev (10^{-6} SI)	$P_j \pm$ stdev	σ_{K_1} (deg)	σ_{K_3} (deg)
Insizwa mafic sill								
Upper	Qtz-diorite/Qtz-monzonite	UDM	<110	–	–	–	–	–
	upper Ol-Hyp gabbronorite	CUG	190	126	8869 ± 6058	1.045 ± 0.024	37	3.6
	Qtz-Hyp gabbronorite	CQG	150	18	1901 ± 1298	1.063 ± 0.037	3.9	6.0
Central	Ol-Hyp gabbronorite	COG	50	18	1762 ± 562	1.057 ± 0.010	2.4	4.6
	lower Qtz-Hyp gabbronorite	CLQ	70	36	1198 ± 581	1.046 ± 0.024	3.6	6.1
	lower Ol-Hyp gabbronorite	CLO	30	45	756 ± 278	1.032 ± 0.026	11.6	6.9
	plagioclase peridotite	LPE	85	152	4626 ± 3023	1.080 ± 0.112	4.5	5.1
Lower	Ol-Hyp gabbronorite	LOG	15	45	1326 ± 529	1.051 ± 0.070	9.5	7.8
	fine-grained gabbro	LFG	10	3	1527 ± 1083	2.037 ± 1.567	1.4	7.0
		total thickness = 710		Average[b] = 4363				
Contact	hornfels	HOR	5 to 30	42	404 ± 397	1.032 ± 0.026	22.7	8.1
	granophyre	GRA	<10	16	1307 ± 666	1.019 ± 0.010	6.3	11.9
Other mafic bodies								
Taylor's Koppie Dike	gabbronorite	TKD	<500	153	2479 ± 5236	1.054 ± 0.063	9.5	8.9
Sills, dikes	dolerite	DOL	10 to 100	45	5742 ± 28.07	1.051 ± 0.030	3.2	2.4

[a] From Scholtz (1937).
[b] Average weighed by thickness.

Table 2. Magnetic susceptibility and AMS data of the Insizwa rocks

No	Unit code	K_m 10^{-6} SI	P_j	T_j	Magnetic		StErr	σ_{K_1}	σ_{K_3}	α_{K_1}	α_{K_3}	n
					Lineation	Foliation						
1	TKD	2308	1.133	0.0	116/33	150 E 47	2.02	2	3	17	11	18
2	LPE	8631	1.055	0.2	293/33	112 N 87	0.79	11	7	12	11	11
3	LPE	2079	1.043	−0.3	303/9	118 N 71	1.19	4	6	22	17	12
4	LPE	2059	1.048	−0.1	315/8	94 N 15	1.40	3	6	10	18	12
5	LPE	5523	1.063	0.0	322/45	149 W 79	0.40	11	24	20	17	12
6	COG	2260	1.053	0.4	112/43	119 N 83	0.68	3	1	7	3	9
7	CLO	916	1.032	0.2	309/6	135 W 4	3.74	19	15	47	35	9
8	TKD	944	1.058	0.1	267/2	147 W 5	0.78	3	2	13	11	9
9	COG	1264	1.062	−0.4	115/12	103 S 45	1.09	2	8	12	30	9
10	CUG	6563	1.055	0.0	311/7	126 S 65	0.74	3	4	37	53	9
11	CUG	24,445	1.076	0.6	130/9	90 S 14	0.60	3	1	10	9	9
12	DOL	1480	1.056	0.1	356/70	92 N 70	0.68	2	1	5	11	9
13	HOR	720	1.062	0.5	154/1	38 W 7	1.24	21	15	50	30	9
14	CQG	764	1.033	0.1	315/11	116 S 76	1.09	6	11	44	42	9
15	CUG	3874	1.087	−0.4	153/88	105 S 89	0.63	1	2	6	11	9
16	CUG	4400	1.031	0.5	147/69	120 S 78	0.49	6	2	31	9	9
17	CUG	9689	1.017	0.0	310/28	116 N 51	0.46	5	5	45	36	9
18	CUG	14,823	1.055	−0.4	110/65	164 E 67	0.74	1	3	9	23	9
19	CUG	14,029	1.061	−0.4	247/42	109 S 53	0.98	1	4	9	16	9
20	CUG	9436	1.034	−0.2	158/17	151 W 63	0.53	3	8	29	38	9
21	TKD	599	1.019	0.2	102/3	75 S 18	1.02	16	10	42	38	9
22	LOG	1598	1.015	−0.4	290/16	118 S 48	0.53	11	14	30	42	9
23	TKD	1568	1.176	0.4	133/10	28 E 11	2.15	3	1	17	20	9
24	TKD	1640	1.045	−0.1	133/25	131 S 89	1.12	3	4	9	30	9
25	TKD	688	1.003	0.2	120/30	119 N 89	0.47	22	14	25	7	9
26	TKD	765	1.008	−0.4	133/4	82 S 8	1.42	16	35	15	22	9
27	TKD	729	1.004	0.4	172/27	141 W 46	0.57	29	15	45	46	9
28	TKD	1629	1.017	−0.2	138/60	169 E 70	0.64	7	8	26	39	9
29	TKD	19,265	1.040	0.0	133/40	2 E 49	0.47	2	4	9	12	9
30	TKD	1056	1.035	0.1	289/37	56 N 44	1.60	12	8	26	32	9
31	DOL	5887	1.030	0.0	99/27	110 N 69	0.55	3	3	52	54	9
32	TKD	650	1.005	0.1	284/19	30 W 23	0.55	15	15	43	17	9
33	LPE	752	1.044	0.2	305/1	115 N 86	1.06	3	2	31	33	9
34	LPE	622	1.020	0.3	103/7	104 N 81	0.61	6	3	12	10	9
35	CLO	585	1.016	−0.1	116/16	125 N 64	0.53	5	5	9	15	9
36	CLO	1182	1.078	0.6	111/34	111 S 90	1.14	6	1	8	3	9
37	CLQ	781	1.073	0.0	343/13	85 N 11	2.19	4	6	41	38	9
38	CLQ	919	1.047	−0.1	117/18	107 S 53	0.87	3	4	14	26	9
39	CLQ	1844	1.044	−0.5	111/9	120 N 39	0.74	2	8	9	27	9
40	CQG	3037	1.098	0.2	324/18	143 E 86	1.03	2	1	11	9	9
41	CUG	3940	1.027	0.1	129/8	130 N 84	0.37	4	3	12	11	9
42	LOG	412	1.007	0.1	274/52	163 W 48	0.51	20	13	50	48	9
43	LPE	961	1.096	0.1	128/27	1 E 32	0.67	1	1	11	8	9
44	TKD	3575	1.191	−0.4	53/54	114 N 61	1.81	1	2	37	18	9
45	TKD	2030	1.030	−0.1	107/52	91 S 78	0.66	7	4	27	12	9
46	LOG	1547	1.184	0.7	169/50	179 E 77	1.72	5	1	26	20	9
47	LPE	4018	1.419	0.7	341/52	120 N 61	2.58	5	1	39	5	9
48	LPE	4762	1.039	0.1	274/3	94 N 88	0.87	5	4	18	13	9
49	CLO	427	1.013	0.2	329/5	178	0.82	15	10	16	11	9
50	DOL	6335	1.036	0.5	169/60	130 S 72	0.57	6	1	41	10	9
51	LPE	2707	1.029	−0.1	118/20	172 E 19	0.96	5	5	39	48	9

Table 2 (*continued*)

No	Unit code	K_m 10^{-6} SI	P_j	T_j	Magnetic		StErr	σ_{K_1}	σ_{K_3}	α_{K_1}	α_{K_3}	n
					Lineation	Foliation						
52	LOG	1638	1.024	−0.2	1/2	1 E 78	0.90	6	8	33	35	9
53	CLO	673	1.021	0.6	79/4	81 N 18	0.79	14	3	41	9	9
54	CLQ	1248	1.039	0.2	303/23	138 W 55	0.95	6	6	18	29	9
55	CUG	4402	1.031	0.4	278/52	103 S 87	0.79	7	2	19	4	9
56	CUG	4781	1.030	0.3	326/15	89 N 18	0.79	7	3	19	22	9
57	CUG	10,854	1.040	−0.5	344/73	113 N 77	0.60	2	7	11	28	9
58	CUG	7841	1.034	−0.2	176/72	124 S 80	0.76	3	4	46	42	9
59	CUG	4114	1.029	0.0	317/12	137 E 78	0.65	4	3	32	22	9
60	LOG	1435	1.027	0.3	65/5	52 S 18	0.80	6	3	29	8	9
61	DOL	5235	1.029	−0.2	320/7	146 W 45	0.70	3	5	9	29	9
62	DOL	9771	1.103	0.1	196/81	40 E 86	1.14	2	2	4	15	9
63	TKD	1528	1.017	−0.3	150/29	112 S 57	0.85	10	12	46	35	9
64	TKD	861	1.011	0.0	334/61	109 N 51	1.05	12	11	39	29	9
65	LPE	5811	1.061	−0.3	308/28	87 N 34	0.55	1	2	24	34	6
66	LPE	7958	1.123	0.3	124/35	126 N 88	1.25	1	1	2	2	6
67	LFG	1527	2.460	0.8	325/6	123 S 86	11.30	7	2	44	34	3
68	LPE	7689	1.089	0.3	10/42	61 N 50	1.04	3	2	3	3	4
69	HOR	296	1.005	0.4	203/79	59 S 86	2.00	53	28	24	7	3
70	LPE	7888	1.033	−0.2	332/61	148 E 87	0.75	2	3	3	4	10
71	LPE	8095	1.059	−0.4	49/21	73 N 44	1.16	1	3	2	4	7
72	LPE	8890	1.029	0.1	308/74	152 W 84	0.50	4	3	8	6	7
73	HOR	298	1.023	0.7	327/22	124 N 43	1.00	27	5	44	33	18
74	GRA	1307	1.022	−0.1	172/49	74 S 53	0.81	6	12	15	36	16
75	LPE	8161	1.053	0.1	330/59	138 E 83	1.32	3	2	2	3	6
76	LPE	1565	1.111	0.5	306/46	2 W 52	1.63	3	1	2	3	5
77	HOR	325	1.047	0.6	8/8	66 N 10	1.83	11	2	9	10	9
78	HOR	431	1.040	0.5	290/29	136 W 55	1.23	10	4	35	40	3
											total = 699	

See Fig. 2 for AMS station localization. Underlined numbers have been removed from structural datasets.

Within the Insizwa mafic sill, the average magnetic susceptibility K_m of individual stations ranges from 412 to 24,445×10^{-6} SI. The average susceptibility, calculated on 443 specimens and weighed by unit thickness, is 4363×10^{-6} SI. The within-unit K_m variation is large (20–70%). The Lower Zone displays susceptibilities around 4600×10^{-6} SI, except for the lower Ol-Hyp gabbronorite (LOG) and the lower fine-grained gabbro (LFG) which have lower susceptibilities around 1500×10^{-6} SI. In the Central Zone, the magnetic susceptibility increases from base to top, from 750 to 12,000×10^{-6} SI. Overall, variations in the magnetic susceptibility depend mostly on the stratigraphic position of the samples. Lateral variations of K_m in map view cannot be delineated due to the large within-unit variability. The magnetic susceptibility shows a multimodal distribution with peaks corresponding to some of the main units: CLO≈750×10^{-6} SI, CQG+COG×1700×10^{-6} SI and CUG≈4800×10^{-6} SI.

In the contact zone, hornfels show the lowest magnetic susceptibilities of all units (≈400×10^{-6} SI). These values are significantly higher than those of unmetamorphosed Karoo sandstones and shales (<150×10^{-6} SI, Maré and Ousthuizen, 2000). Granophyres exhibit a wide range of magnetic susceptibilities from 700 to 3500×10^{-6} SI.

Rocks from the Taylor's Koppie dike also show a wide range of magnetic susceptibilities from 600 to 4000×10^{-6} SI with high values in station 29 in which 25,000<K_m<30,000×10^{-6} SI. Dolerites have average magnetic susceptibilities around 6000×10^{-6} SI, i.e. higher than both the Insizwa mafic sill and the Taylor's Koppie dike.

4.2. Degree of anisotropy and ellipsoid shape

The degree of magnetic anisotropy P_j (Table 1 and Table 2, Fig. 5 and Fig. 6) is moderate, less than 1.10 in 75% of specimens and 90% of stations. Within-core variation of P_j is <30% in 86% of cores and within-station variation of K_m is <30% in 70% of stations. One mineralized station from the LFG unit (#067) has very large anisotropies, between 1.30 and 3.00, and has been excluded from the following statistics.

In the Insizwa sill, P_j ranges from 1.007 to 1.070 with a median value around 1.044. The within-unit variation of P_j ranges between 30% and 100%. The Lower Zone Ol-Hyp gabbronorite (LOG) generally has low P_j, from 1.007 to 1.027. The Lower Zone plagioclase peridotite (LPE unit) displays anisotropies between 1.02 and 1.10. In the Central Zone, anisotropies remain low to moderate except in the Qtz-Hyp gabbronorite (CQG unit) where P_j reaches nearly 1.10. In summary, P_j does not correlate tightly with the stratigraphic height in the intrusion. No particular lateral variations of P_j (in map view) have been delineated.

In the contact zone, granophyres display low to moderate anisotropies (≈1.02) and hornfels display moderate P_j values (1.02–1.05). Finally, gabbronorites from the Taylor's Koppie dike and dolerites show highly variable P_j values, ranging from 1.005 to 1.20.

Specimens from the Insizwa sill show two trends of positive correlation between P_j and K_m (Fig. 5). The main group is characterized by a low anisotropy (P_j<1.10) gently increasing with increasing K_m. This is particularly clear on in Fig. 5A in the entire range of K_m values. The lower limit for P_j is most likely controlled by the intrinsic anisotropy of the dominant minerals. The other group of specimens shows a steep increase of P_j for a small increase of K_m (Fig. 5B).

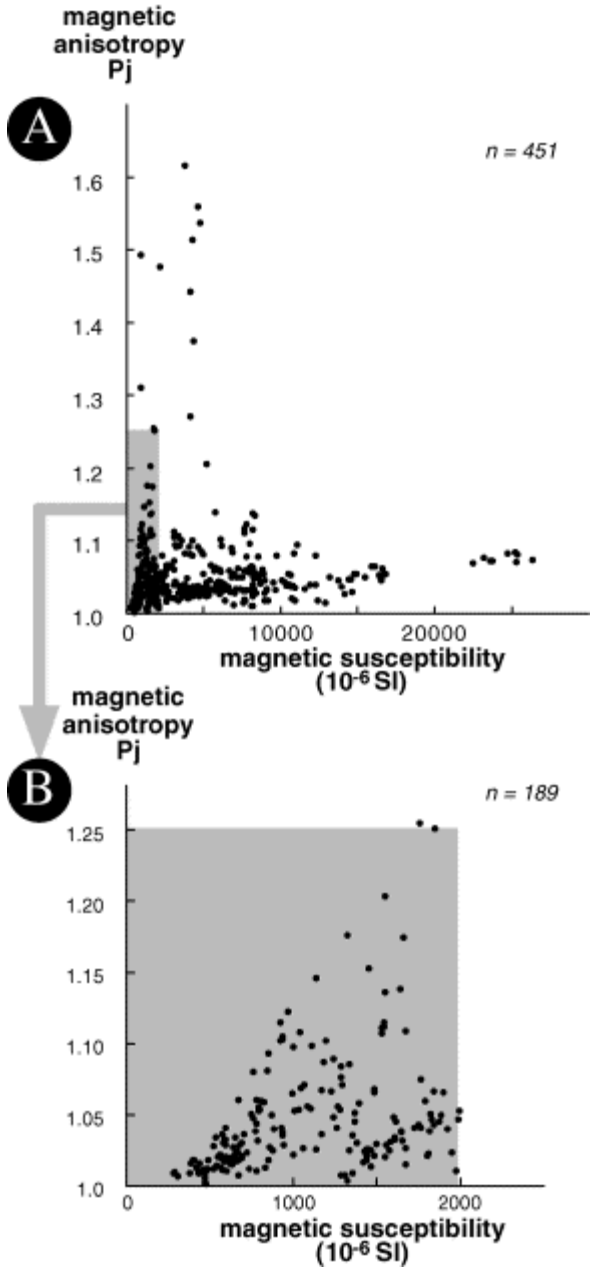

Fig. 5. (A) Plot of magnetic anisotropy P_j vs. magnetic susceptibility (10^{-6} SI). The diagram shows two trends corresponding to large increase of anisotropy in the low susceptibility range and small increase of anisotropy in the whole susceptibility range. The lack of increase of P_j with K at high susceptibilities strongly suggests that distribution anisotropy (proportional to cube of distance between interacting particles) does not occur. (B) Detail of the low K range.

The shape of the magnetic fabric ellipsoid (oblate or prolate) does not correlate with the magnetic susceptibility or with the stratigraphic height in the Insizwa sill. However, specimens from the CLO unit have more oblate ellipsoids than the other units (Table 2). Pyrrhotite-bearing specimens have strongly oblate magnetic ellipsoids (T_j≈0.8) and P_j>1.20 (Fig. 6).

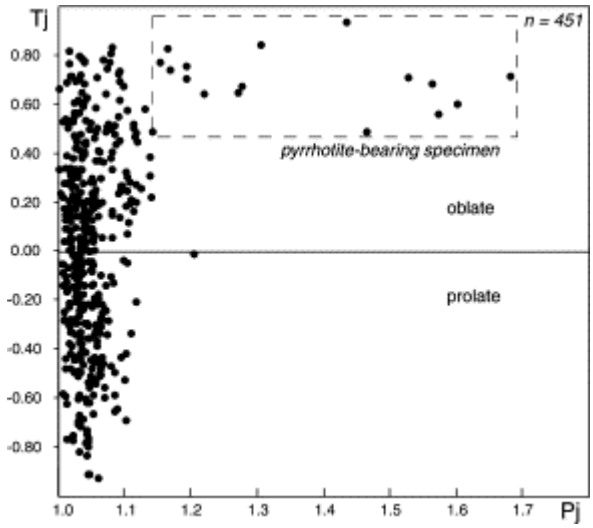

Fig. 6. Plot of shape factor T_j vs. degree of anisotropy. No preferred relationship between the two parameters exists except for pyrrhotite-bearing samples characterized by a high P_j (which is an intrinsic property of pyrrhotite).

4.3. Identification of magnetic minerals

The main ores were identified first by reflected light microscopy on core specimens in order to select samples for further investigation with thermomagnetic and high-field methods. Magnetite (Mt) and ilmenite occur throughout the Insizwa sill and generally form euhedral, elongated and tabular grains, usually >200 μm, highly disseminated in the silicate gangue. They are interpreted as primary magmatic grains. Pyrrhotite (Po), chalcopyrite and pentlandite, restricted to the Lower plagioclase peridotite unit (LPE) and units below, are anhedral and interpreted as primary magmatic sulfides. Large magnetite grains (>100 μm) are seldom in the Lower Zone and the lowermost unit of the Central Zone (CLO).

Samples for thermomagnetic experiments were prepared from crushed rock fragments (≈1 mm diameter). Experiments ran under natural atmosphere, i.e. oxidizing conditions, in both Mt only and Mt+Po units. The Curie temperature (T_c) of the Mt-bearing samples is typically at 510±10 °C which indicates a titanomagnetite with composition x_{ulv}≈0.114±0.015. Heating and cooling curves were similar. By contrast, experiments on the Mt+Po-bearing samples were not reversible due to thermally induced reactions between sulfides and iron oxides (Fig. 7A). The absence of a substantial decrease in magnetic susceptibility at about 250–300 °C on the heating curves suggests that the contribution of magnetite to the susceptibility is larger than that of pyrrhotite. On the cooling path, the composition and amount of magnetite may have changed due to the reducing conditions created by the breakdown of pyrrhotite in SO_2. These results conform with the thermal demagnetization data of Hattingh and de Wet (1996) on the Insizwa rocks which also indicate the dominance of magnetite.

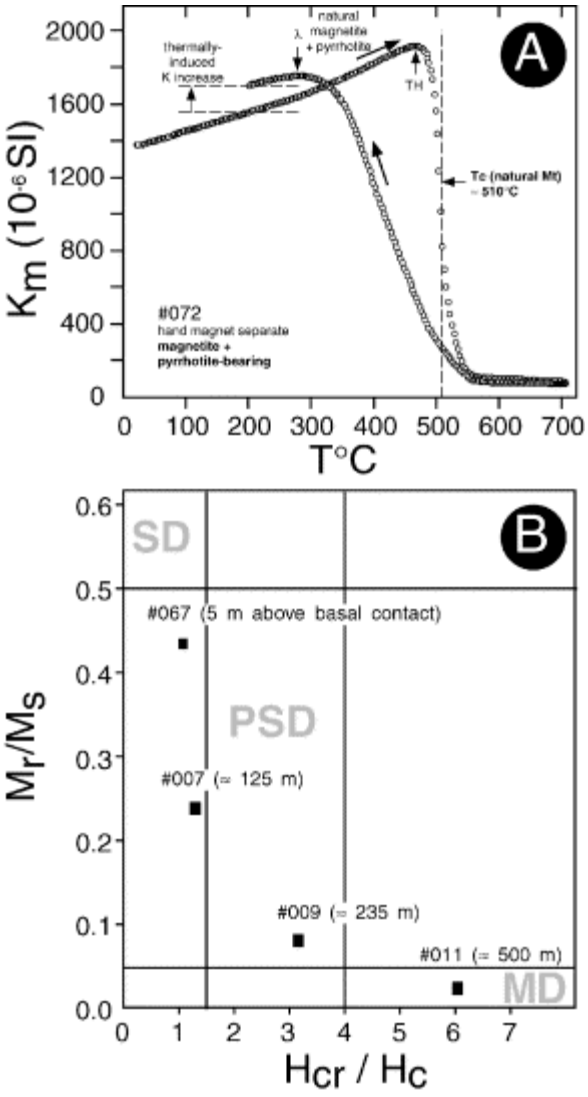

Fig. 7. (A) Thermomagnetic experiment of sample #072 containing both magnetite and pyrrhotite. The nonreversible nature of the experiment results from heating induced reaction. (B) Magnetic domain grain sizes of four representative samples at different heights in the Insizwa sill. See Table 2 and Fig. 2 for positions.

Hysteresis properties were determined in high-field on three Mt samples and one Mt-Po sample coming from several units (LFG, CLO, COG and CUG). The hysteresis properties suggest an upward increase of domain-size from single-domain to multidomain (Fig. 7B). The low H_{cr}/H_c ratios of the lower two samples (#067 and #007), together with their low susceptibility (1500 and 900×10^{-6} SI, respectively) and the scarcity of large magnetite grains, are consistent with magnetite occurring mostly as single-domains submicroscopic exsolutions in the lattice of mafic silicates. Palaeomagnetic investigations of Hattingh and de Wet (1996) on the Insizwa rocks also indicate the presence of SD magnetite grains in the lower parts of the Insizwa sill.

The following paramagnetic contributions ($K_{p\text{-meas}}$) of three representative samples was deduced from measurements of the high-field magnetization slope, above saturation.

Unit	Station #	$K_{p\text{-meas}}$ (10^{-6} SI)	% paramagnetic susceptibility
COG	9	626	50
CUG	11	607	2
LFG	67	817	50

4.4. Magnetic lineations and foliations

A total of 20 stations out of 78 (gray in Fig. 8), marred by large uncertainties, have been removed from the structural datasets for either one of the following reasons.

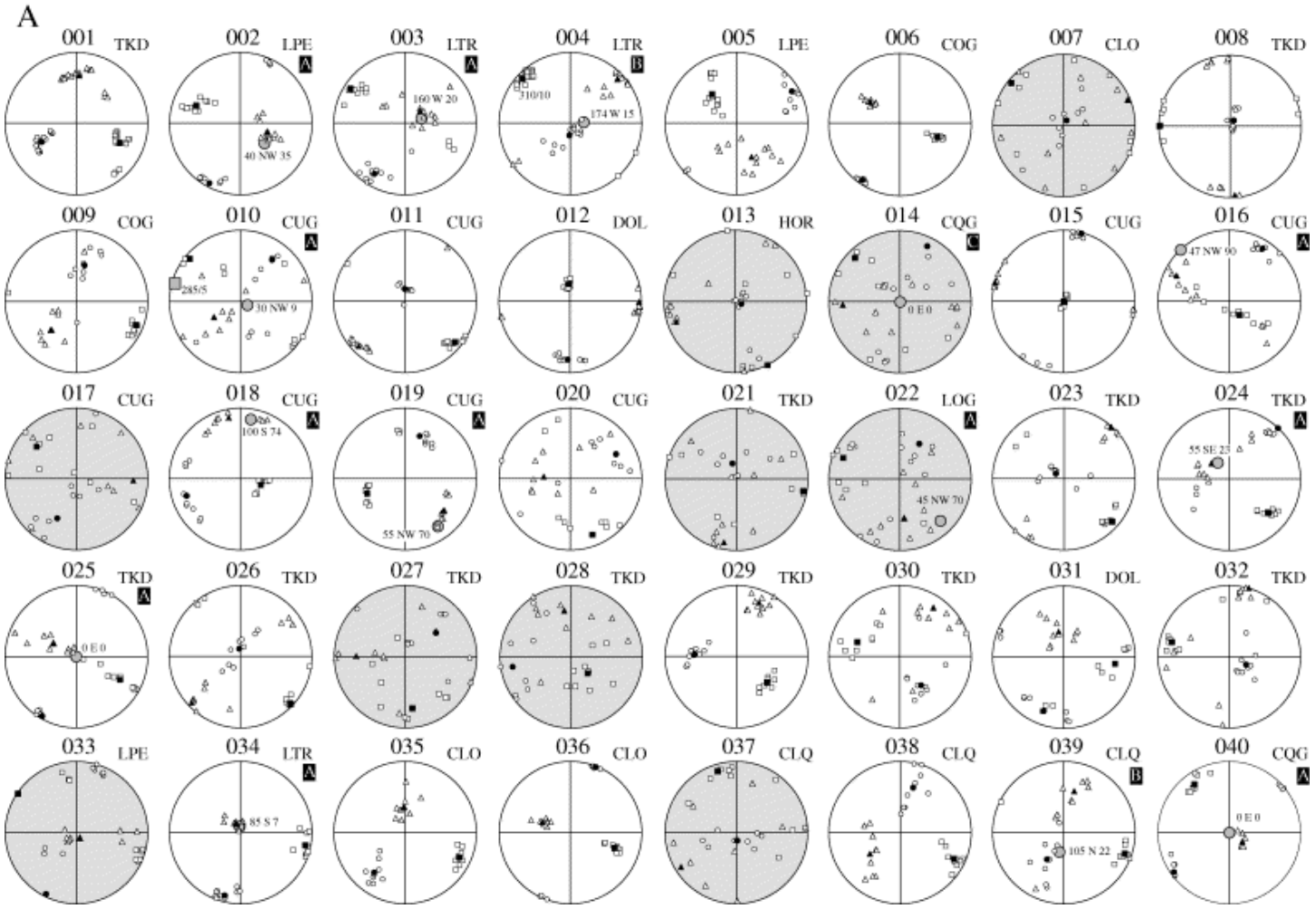

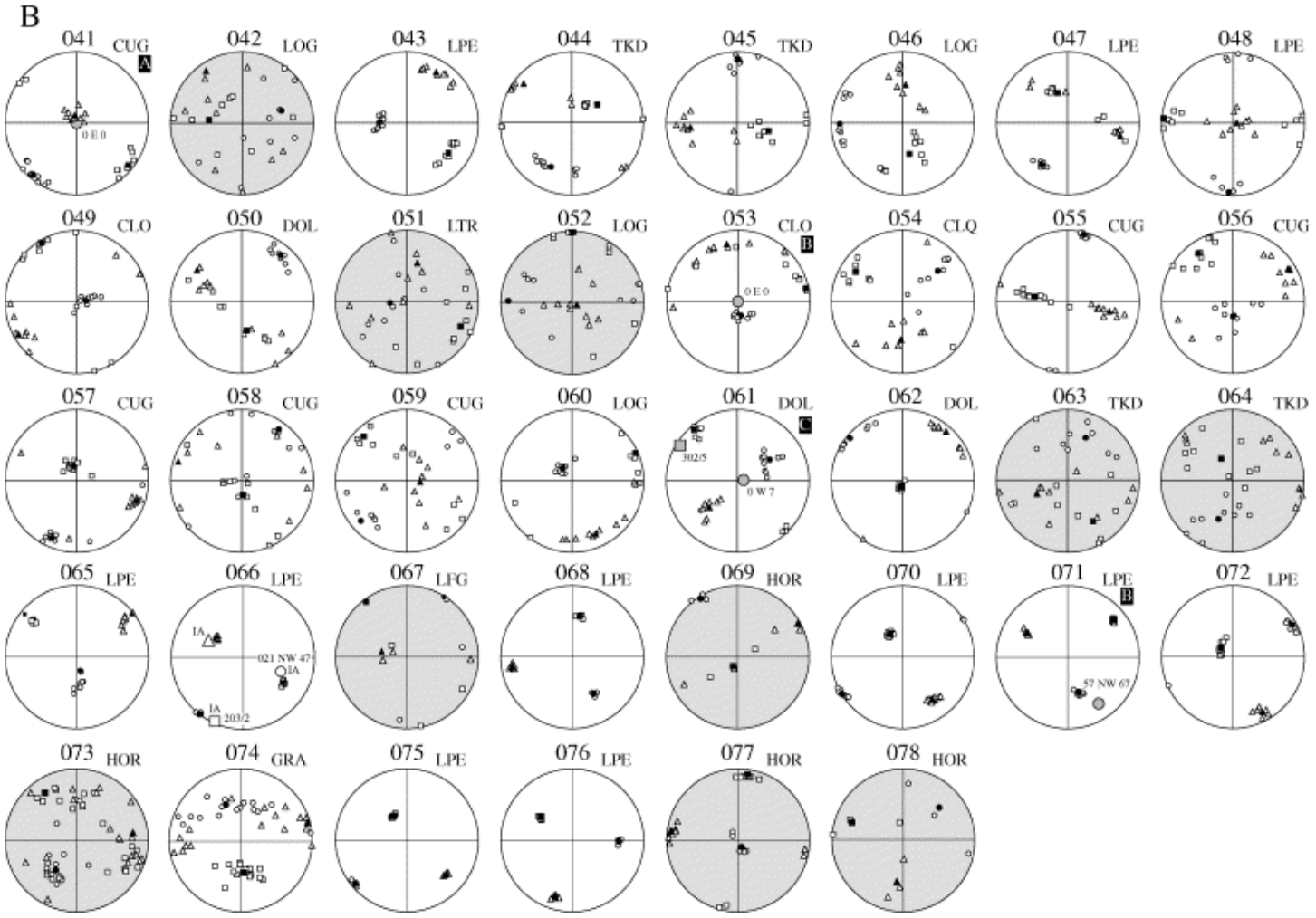

Fig. 8. Stereonets of the magnetic fabrics including K_1, K_2 and K_3 axes (white symbols) and averages (black symbols). Stations with grayish stereonets have been discarded from the structural dataset for reasons explained in the text. White letters on black background indicate magnetic fabric types. Field measurements are indicated with gray symbols. Image analysis axes for station #066 are labeled with IA.

1) The analytical error and the measurement departures from an ellipsoid are represented by the standard error (StErr in Table 2). Stations #007 and #067 (massive sulfide) have been discarded because they have StErr>3.

(2) σK_i is larger than 25°—The error on the determination of the ellipsoid axes is given by σK_i, the 95% confidence half angle of each axes (i=1–3). σK_i are given in Table 1 per unit and in Table 2 per station. In the Insizwa sill, σK_1 and σK_3 are usually better than 6° except in the lower parts of the Central Zone (CLO) and of the Lower Zone (LOG, LFG). Dolerites generally have well defined fabrics with σK_1 and σK_3 around 3°. Hornfels, granophyres and the Taylor's Koppie dike rocks have the highest σK_1 and σK_3. For stations such as #069 where the number of specimens is small (n=3), the results cannot be considered meaningful.

(3) αK_i>25°—The within-station fabric variability is given by the αK_i angle, which is the average departure of the specimens vectors from the mean station vector. These values are given in Table 2 for K_1 and K_3 axes. Only 56% of stations have an αK_1<25° and 59% have an αK_3<25°.

Out of the 58 remaining stations, 41 stations belong to the Insizwa sill and 11 to the Taylor's Koppie dike. Overall, the magnetic lineation is consistent at various scales: Waterfall Gorge Mine, Target D area and the whole area (Fig. 10A). The sill (41 stations, 360 specimens) has a NW–SE subhorizontal magnetic lineation (K_1) with eigen vector at 304°, 5° (Fig. 9 and Fig. 10). The magnetic foliation, shown as pole (K_3) in Fig. 8 and Fig. 9, defines a NW–SE strike and a NE steep dip best foliation at 124° NE 83° (Fig. 9 and Fig. 10). The dike (11 stations, 108 specimens) defines a similar magnetic lineation (K_1) with a similar NW–SE but slightly steeper plunge, with eigen vector at 117°, 20°. The magnetic foliation strikes dominantly NW–SE with steep dip. In a few localities, the foliation strikes NE–SW with a gentle southerly dip (Fig. 10B).

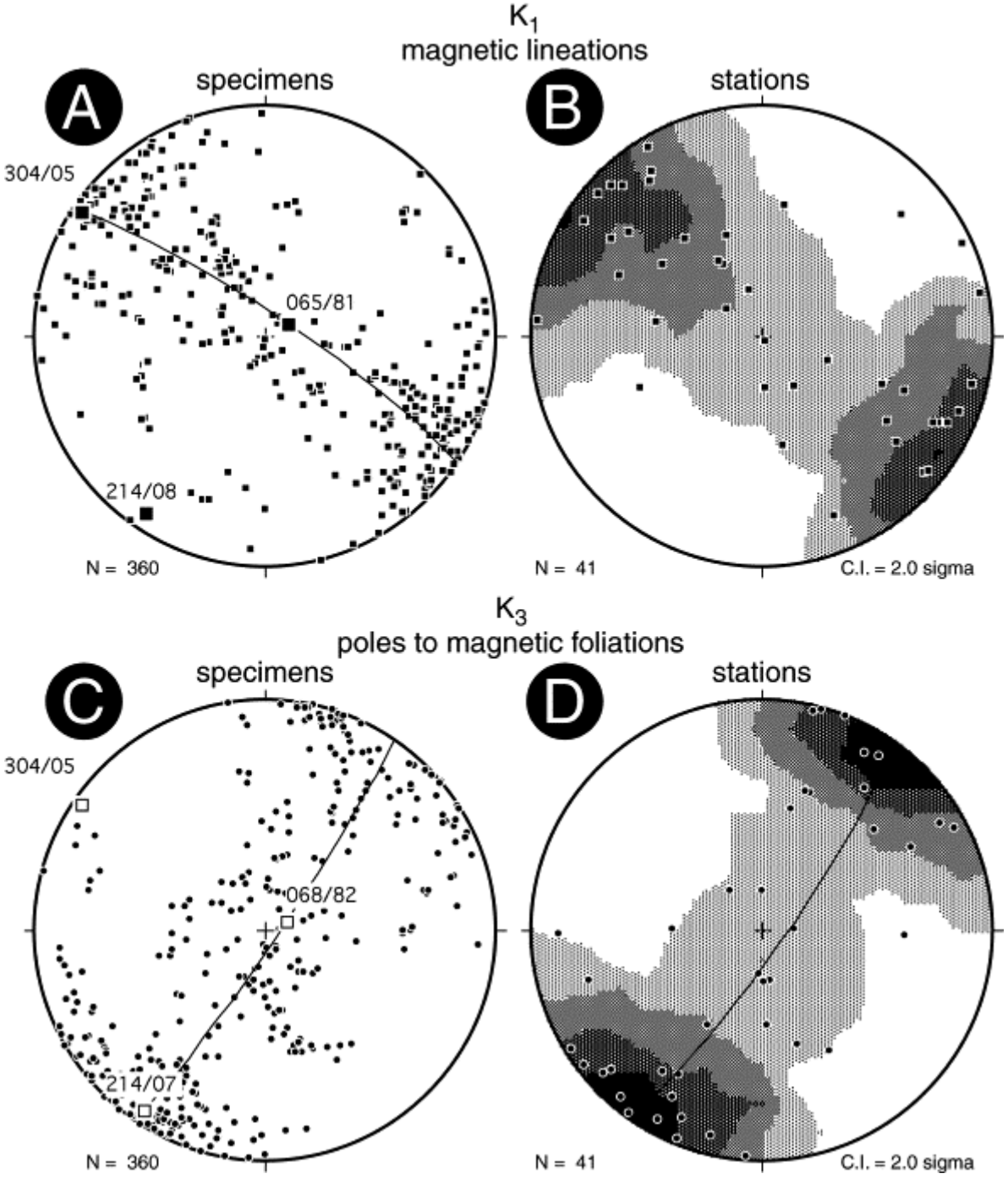

Fig. 9. Stereonets of magnetic fabrics for the Insizwa sill only. (A) Lineations for specimens. (B) Lineations for stations (with contours). (C) Foliations for specimens. (D) Foliations for stations (with contours). Eigen vectors of the distributions are plotted with larger symbols. Stereonet software of Allmendinger (1992).

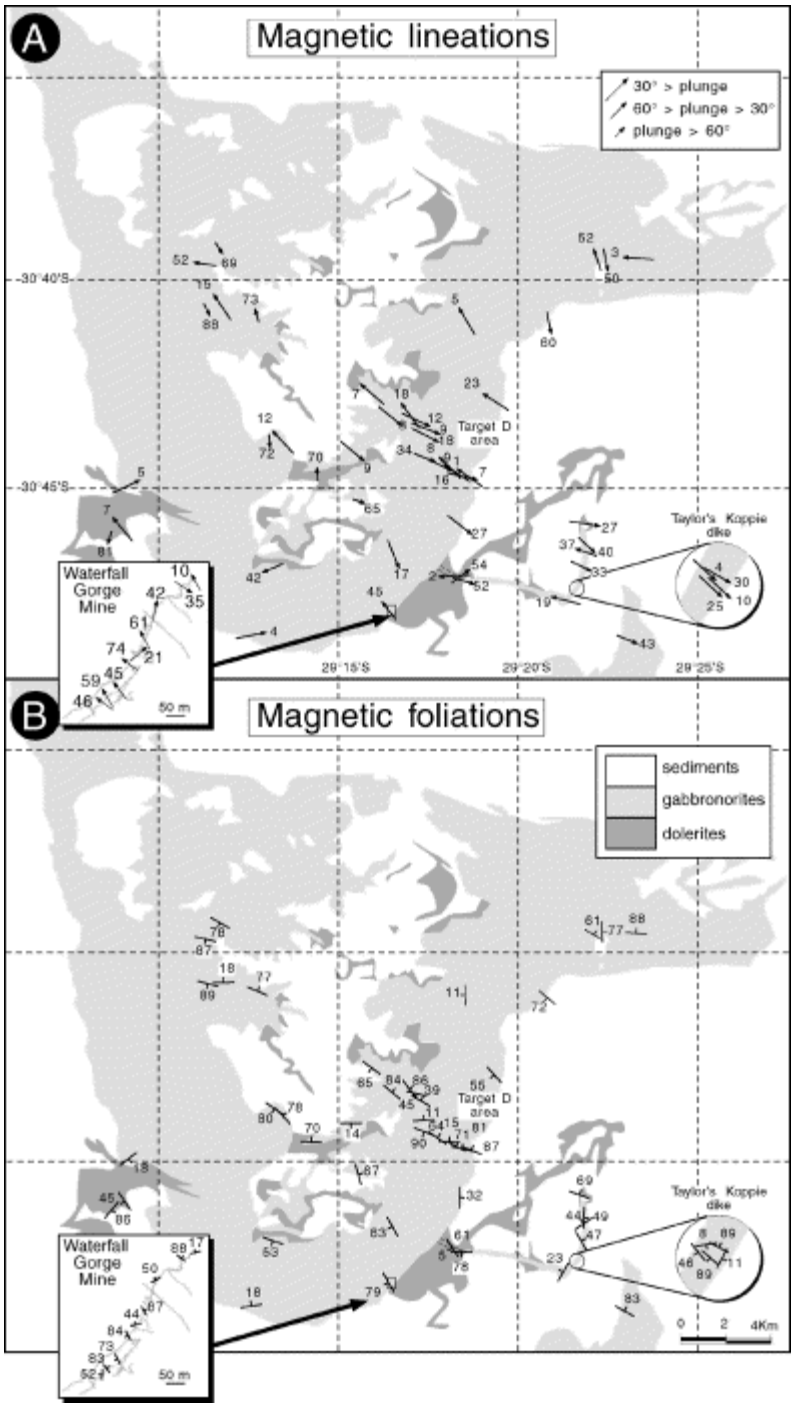

Fig. 10. Maps of magnetic structures in the Insizwa area. (A) Magnetic lineations. (B) Magnetic foliations. Insets: Details of structures at the Waterfall Gorge Mine.

5. Discussion

5.1. Origin and significance of mesoscopic field structures

The processes responsible for the formation of a compositional layering in mafic intrusions are multiple (Naslund and McBirney, 1996) but they are dominated by gravity and flow forces. Gravity causes crystal settling which results in the formation of horizontal layered cumulates (Nicolas, 1992). Flow forces cause

the preferred orientation of anisotropic particles, according to which the tabular crystal faces subparallel to the layering will form a magmatic foliation (McBirney and Nicolas, 1997). The slight obliquity between the flow plane and magmatic foliation is attributed to the process of imbrication (Den; Blanchard and Knight).

At Insizwa, we interpret structures formed by primary magmatic minerals as pristine magmatic structures. Furthermore, the Karoo Basin in the Insizwa area did not record any deformation (e.g., Eales et al., 1984) after the emplacement of the Insizwa sill at 183±1 Ma (Duncan et al., 1997). This agrees with the magmatic microstructure of the rocks, as observed under the microscope, and with the relatively low magnetic anisotropies (P_j<1.10). Field data (18 measurements, Fig. 8), borehole data and the overall dish shape of the Insizwa sill suggest that the compositional layering is subhorizontal except near the margins of the sill. The foliation, generally marked by plagioclase, is parallel to the layering and interpreted as representing the magma flow plane.

At Insizwa, readings of the magmatic lineation are few (3 measurements, Fig. 8) but unambiguous. The mineral lineation lies within the layering-foliation plane and is interpreted as parallel to the magma flow direction.

5.2. Source of the magnetic susceptibility

Interpretation of magnetic fabrics requires preliminary quantitative assessment of the contributions of individual phases to the bulk magnetic susceptibility. The three contributions, diamagnetic, paramagnetic and ferromagnetic, are discussed successively in the following.

The diamagnetic contribution originates from plagioclase which, with an intrinsic magnetic susceptibility of -2.78×10^{-6} SI (Borradaile et al., 1987), is negligible.

The paramagnetic contribution is mostly from Fe^{2+}, Fe^{3+} and Mn^{2+} in ferromagnesian silicates (olivine, pyroxene, biotite). The maximum theoretical paramagnetic susceptibility ($K_{p\text{-}theor}$) is calculated using the following formula (Syono and Rochette):

$$K_{p\text{-}theor}=d/1000\times(25.2\times Fe^{2+}+33.4\times Fe^{3+}+33.8\times Mn^{2+})$$

with d=density of rock and Fe^{2+}, Fe^{3+} and Mn^{2+} in wt.%.

Using the density measurements of Sander and Cawthorn (1996), the chemical analyses of Eales et al. (1984), and assuming a 85%/15% partition of FeO/Fe_2O_3, which is typical of mafic liquids (Sack et al., 1980), we obtain $K_{p\text{-}theor}$=750 to 1250×10^{-6} SI for the peridotite to gabbronorite suite of Insizwa. These values are larger than the measured susceptibilities because part of the iron contributes to form ferromagnetic species (Mt, Po).

The ferromagnetic contribution originates chiefly from magnetite as shown by reflected light microscopy and by thermomagnetic experiments. Pyrrhotite-bearing samples are distinguished by oblate magnetic ellipsoids (T_j>0.5), which result from the intrinsic anisotropy of pyrrhotite (Tarling and Hrouda, 1993), and large anisotropies (P_j>1.06). Since the diamagnetic contribution is negligible, the difference between the measured magnetic susceptibility (Table 2) and the calculated paramagnetic susceptibility corresponds to the ferromagnetic susceptibility only. In the Mt-bearing samples #009 and #011, the ferromagnetic

contribution corresponds to a volume of magnetite of 0.02% and 0.85%, respectively (considering intrinsic K_{Mt}≈2.8 SI, Borradaile and Henry, 1997). In the Po+Mt-bearing sample #067, the ferromagnetic contribution would correspond to a volume of magnetite+pyrrhotite of 0.02–0.05% (considering intrinsic K_{Po}≈1.5 SI; Borradaile and Henry, 1997). In summary, the magnetic susceptibility of most rock types is controlled by ferromagnetic phases (Mt and Po) representing small volumes of the rocks (0.02–0.85%).

5.3. Origin of the AMS fabrics

The magnetic lineations, represented by the K_1 axes in Fig. 8A and B coincide with the mineral lineation in all three stations where it could be measured (#4, 10 and 61). At the scales of the whole Insizwa intrusion, of the Target D area and of the Waterfall Gorge Mine, the magnetic lineation is very consistent both in trends and shallow plunges (Fig. 10A). We interpret the NW–SE trending magnetic lineation as the magma flow direction. This is consistent with magma flowing from the SE of Insizwa, where the less differentiated lobes of the Mount Ayliff Complex are situated, lobes which are also at a lower stratigraphic level in the Karoo sedimentary sequence.

The magnetic foliation, represented by the plane normal to K_3 axis, is on average subvertical and therefore broadly perpendicular to the subhorizontal layering (Fig. 9 and Fig. 10). Three configurations of the relationship between the magnetic axes and the magmatic foliation are observed (Fig. 8, labels A, B or C):

the magmatic foliation pole coincides with K_2 magnetic axis (12 out of 18 stations);

the magmatic foliation pole coincides with K_3 magnetic axis (4 out of 18 stations);

the magmatic foliation pole plots in-between K_2 and K_3 axes (2 out of 18 stations).

We see no correlation between the type of configuration and rock unit, geographic position, or K_m, P_j, T_j and StErr parameters. Configuration A is not only the most frequent but also corresponds to the general strike of magnetic foliations (Fig. 9A). Therefore, we suggest that this “intermediate” configuration (Rochette et al., 1999) would also apply to stations of type A for which the foliation was not visible, and reflects a fundamental character of these mafic rocks. Similar difficulties in interpreting AMS fabrics have been encountered by others, both in dikes and sills (see Cadman et al., 1992). In the following, we discuss some of the possible causes for the discrepancy between magmatic and magnetic foliations, i.e. the origin of “intermediate fabrics”.

(i) The *imbrication* of magnetic foliations, initially reported by Knight and Walker (1988), occurs when the magnetic foliation plane is oblique to the flow plane (Fig. 11A), usually along dike walls, within one meter from the contact. The angle between the two planes is in general less than 30° (see Tauxe, 1998) with their intersection being perpendicular to the flow direction. At Insizwa, this intersection is parallel to the flow direction and therefore the observed magnetic fabrics cannot result from imbrication.

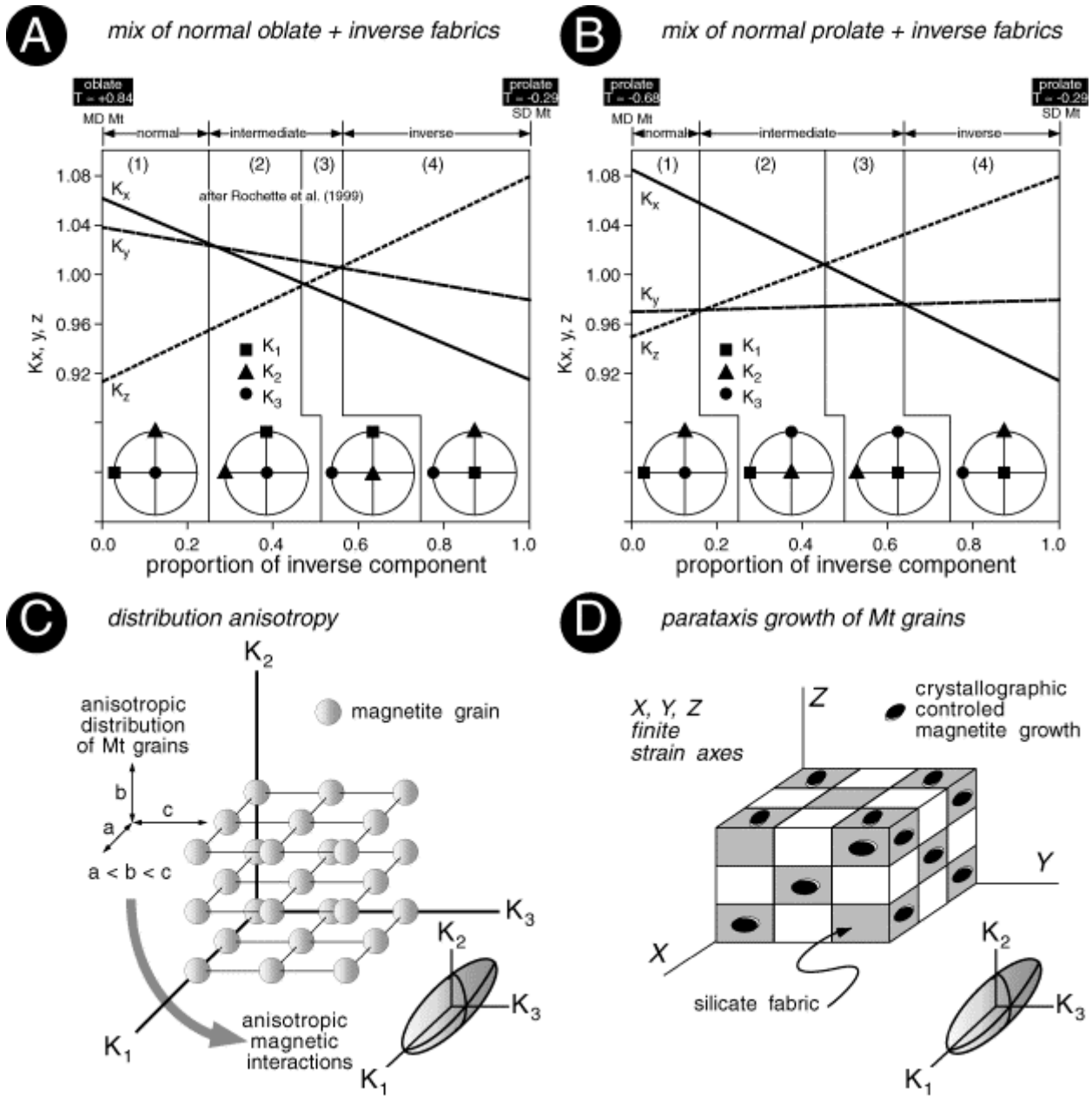

Fig. 11. Models of intermediate magnetic fabrics. (A) Model of Rochette et al. (1999) considering a mix of oblate MD magnetite and prolate SD magnetite. (B) Model considering a mix of prolate MD magnetite and prolate SD magnetite. (C) Model of distribution anisotropy from Hargraves et al. (1991). (D) Model of parataxis growth of magnetic grains in late magmatic melt extraction pockets. The growth is guided by a silicate template, possibly along plagioclase chains.

(ii) *Dominance of single-domain (SD) magnetite* crystals which have their long crystal axis parallel to K_3 (Potter and Stephenson, 1988) which results in fabric inversion (Rochette et al., 1999). Hence, intermediate fabrics may arise in rocks that contain both SD (inverse) and MD (normal) magnetites. The theoretical model of Rochette et al. (1999) does not account for intermediate fabrics in which the K_1 axis remains unchanged because the model is built on a "normal" oblate magnetic ellipsoid (T≈+0.84; Fig. 11A). A different model, built on a "normal" prolate magnetic ellipsoid (T≈−0.68; Fig. 11B) accounts for fabrics in which K_1 is unchanged with a swap between K_2 and K_3 axes. Note that both models assume anisotropy degrees P_j of 1.14 for the normal component, P_j=1.23 for the inverse component and that T=−0.29 for the SD magnetite grains.

The configuration of sample #066 (Fig. 4) could be interpreted as an intermediate fabric similar to case 2 of Rochette et al. (1999) or to case 3 of this study. The abundance of SD magnetite in the plagioclase peridotite (Fig. 7B) supports rather the second possibility.

(iii) *Distribution anisotropy* affecting PSD or MD grains (Hargraves and Stephenson) might be responsible for a magnetic foliation perpendicular to the flow plane. This would require that the magnetite grains would form clusters at distances lesser than grain size and simultaneously that the same grains would be more widely spaced along the finite strain *Y*-axis (Fig. 11D). Such a configuration may arise in a few stations but it is unlikely to be repeated within rock types having different grain sizes and various magnetite contents. In addition, Fig. 5A shows that the increase of P_j with increasing susceptibility is moderate suggesting a minor role played by interactions in the origin of the AMS. Indeed, a number of studies, reviewed in Bouchez (1977), have shown that when K_m increases, the number of magnetite grains increases and the probability for magnetic interactions correlatively increases.

(iv) *Oblique growth of MD magnetite grains* late in the crystallization sequence of gabbronorites and occupying spaces left in the silicate framework. This explains the common association between Fe–Ti oxides and biotite in late-crystallizing fluid-rich melt pockets. The silicate framework, which consists of tabular cumulus plagioclase, olivine and pyroxene, forms a tri-orthogonal fabric (with its *X*-, *Y*- and *Z*-axes) and primarily controls the arrangement of magnetite grains (Fig. 11E). Hypothetically, magnetite grains might have grown along the faces of silicate crystals, a configuration that is referred to in the following as "*parataxis*". The preferred shape of magnetite grains along the *XZ* planes of the silicate framework might result from a two stage process: (1) magma flow at a low crystal/melt ratio forming elongate plagioclase chain network (Philpotts et al., 1999), (2) compaction of the crystal mush, strengthening of a subhorizontal layering and vertical extraction of late-magmatic melt in which magnetite crystallized along with biotite. Step 2 might be contemporaneous with silicate framework retraction on cooling. Fig. 3D (station #16) shows an example of plagioclase veinlets perpendicular to the layering and parallel to the mineral lineation which attest to this magmatic deformation. However, microscopic observations do not support this hypothesis because magnetite grains do not preferentially occur along plagioclase faces.

6. Inferences on magma dynamics and conclusion

A multiple injection is indicated by several cases of angular xenoliths of one unit into another (Fig. 3C). In addition, the magnetic susceptibility increases upward within both the Lower Zone and the Central Zone (Table 1) which also suggests that these zones were formed by distinct magmatic pulses. Finally, unpublished trace element profiles along several boreholes unambiguously support the multiple magma batches hypothesis.

The consistency of the NW–SE trending magnetic lineation in different units points to a uniform flow direction which implies magmatic feeding from a planar feeder (Fig. 1B), i.e. a feeder dike rather than from a pipe (Fig. 1A). The unidirectional flow directions most likely result from a single feeder dike or a set of parallel feeder dikes, as opposed to cross-cutting feeders (Fig. 1C). However, long-lived magmatic systems seem to evolve in time from fissure flow to single vent flow as shown by Wylie et al. (1999). Therefore, our feeding model may not apply to larger mafic sill-like intrusions such as the Bushveld Complex.

Two lines of evidence support the hypothesis that the Taylor's Koppie dike (TKD) acted as a feeder or relay structure for the Insizwa sill: (1) magnetic lineations at TKD plunge towards the least differentiated lobe of

HorseShoe, and (2) the magnetic susceptibility of the TKD rocks is lower than that of the Insizwa sill which may indicate a lesser oxidation degree as expected in a deeper-seated feeding structure.

In conclusion, AMS fabrics are consistent within most stations of the Insizwa sill. The magnetic lineation coincides with the mineral lineation and represents the magma flow direction. The magnetic foliation does not, in general, represent the magma flow plane. The emplacement of the Insizwa sill occurred by multiple injection of differentiated magmas fed from a lower level in the southeast through an oblique relay structure (Taylor's Koppie dike).

Acknowledgements

Falconbridge Venture of Africa provided considerable logistical and financial support for this work. This study was also supported by Rhodes University Research Grant N° 36605-500-105 to Eric Ferré 1998-2000. John Hepple, Wilberforce, Bennet and Chris, technical staff in the Department of Geology at Rhodes University, kindly prepared thin sections and other material for this project. Michel de Saint Blanquat kindly provided his AMS data processing software EX-AMS. The Toulouse magnetic laboratory of UMR CNRS 5563 where all AMS measurements were performed is gratefully acknowledged. Pertinent comments by reviewers Jean Luc Bouchez and Richard Ernst helped in improving the manuscript.

References

Allmendinger, 1992. R.W. Allmendinger , Stereonet, V. 4.52. Program for the Macintosh Computer. (1992).

Blanchard et al., 1979. J.P. Blanchard, P. Boyer and C. Gagny , Un nouveau critère de sens de mise en place dans une caisse filonienne: le “pincement” des minéraux aux épontes. *Tectonophysics* **53** (1979), pp. 1–25.

Borradaile and Henry, 1997. G.J. Borradaile and B. Henry , Tectonic applications of the magnetic susceptibility and its anisotropy. *Earth-Science Reviews* **42** 1–2 (1997), pp. 49–93.

Brown et al., 1994. R. Brown, K. Gallagher and M. Duane , A quantitative assessment of the effects of magmatism on the thermal history of the Karoo sedimentary sequence. *Journal of African Earth Sciences* **18** 3 (1994), pp. 227–243.

Cadman et al., 1992. A.C. Cadman, R.G. Park, J. Tarney and H.C. Halls , Significance of anisotropy of magnetic susceptibility fabrics in Proterozoic mafic dykes, Hopedale Block, Labrador. *Tectonophysics* **207** (1992), pp. 303–314.

Campbell and Griffiths, 1990. I.H. Campbell and R.W. Griffiths , Implications of mantle plume structure for the origin of flood basalts. *Earth and Planetary Science Letters* **99** (1990), pp. 79–93.

Cañón-Tapia et al., 1996. E. Cañón-Tapia, G.P.L. Walker and E. Herrero-Bervera , The internal structure of lava flows-insights from AMS measurements: I—Near-vent a'a. *Journal of Volcanology and Geothermal Research* **70** (1996), pp. 21–36.

Catuneanu et al., 1998. O. Catuneanu, P.J. Hancox and B.S. Rubidge , Reciprocal flexural behaviour and contrasting stratigraphic development model for the Karoo retroarc foreland system. *Basin Research* **10** 4 (1998), pp. 393–408.

Cawthorn et al., 1988. R.G. Cawthorn, S. Maske, M. De Wet, D.I. Groves and K.F. Cassidy , Contrasting magma types in the Mount Ayliff Intrusion (Insizwa Complex), Transkei: evidence from ilmenite compositions. *Canadian Mineralogist* **26** (1988), pp. 145–160.

Cawthorn et al., 1991. R.G. Cawthorn, M. de Wet, C.J. Hatton and K.F. Cassidy , Ti-rich chromite from the Mount Ayliff Intrusion, Transkei: further evidence for high Ti tholeiitic magma. *American Mineralogist* **76** (1991), pp. 561–573.

Chevallier and Woodford, 1999. L. Chevallier and A. Woodford , Morpho-tectonics and mechanism of emplacement of the dolerite rings and sills of the western Karoo, South Africa. *South African Journal of Geology* **102** 1 (1999), pp. 43–54.

Cox, 1988. K.G. Cox , The Karoo province. In: J.D. Macdougall, Editor, *Continental Flood Basalts*, Kluwer Academic Publishing, Norwell (1988), pp. 239–271.

De Decker, 1981. R.H. De Decker , Geology of the Kokstad area. 1: 250,000 geological sheet 3028 Kokstad and explanation. *Geological Survey of South Africa* (1981).

Den Tex, 1969. E. Den Tex , Origin of ultramafic rocks, their tectonic setting and history: a contribution to the discussion of the paper “The origin of ultramafic and ultrabasic rocks” by P.J. Wyllie. *Tectonophysics* **7** 5–6 (1969), pp. 457–488.

Duane and Brown, 1991. M.J. Duane and R.W. Brown , Tectonic brines and sedimentary basins: further applications of fission track analysis in understanding Karoo Basin evolution (South Africa). *Basin Research* **3** (1991), pp. 187–195.

Duncan et al., 1997. R.A. Duncan, P.R. Hooper, J. Rehacek, J.S. Marsh and A.R. Duncan , The timing and duration of the Karoo igneous event, southern Gondwana. *Journal of Geophysical Research* **102** (1997), pp. 18127–18138.

Eales et al., 1984. H.V. Eales, J.S. Marsh and K.G. Cox , The Karoo igneous province: an introduction. *Geological Society of South Africa, Special Publication* **13** (1984), pp. 1–26.

Ellwood, 1978. B.B. Ellwood , Flow and emplacement direction determined for selected basaltic bodies using magnetic susceptibility anisotropy measurements. *Earth and Planetary Science Letters* **41** (1978), pp. 254–264

Encarnacion et al., 1996. J. Encarnacion, T.H. Fleming, D.H. Elliot and H.V. Eales , Synchronous emplacement of Ferrar and Karoo dolerites and the early breakup of Gondwana. *Geology* **24** (1996), pp. 535–538.

Erlank, 1984. A.J. Erlank , Petrogenesis of the volcanic rocks of the Karoo Province. *Geological Society of South Africa, Special Publication* **13** (1984) 395 pp. .

Ernst and Baragar, 1992. R.E. Ernst and W.R.A. Baragar , Evidence from magnetic fabric for the flow pattern of magma in the Mackenzie giant radiating dyke swarm. *Nature* **356** (1992), pp. 511–513.

Ernst and Buchan, 1997a. R.E. Ernst and K.L. Buchan , Giant radiating dyke swarms: their use in identifying preMesozoic large igneous provinces and mantle plumes. *AGU, Geophysical Monograph* **100** (1997), pp. 297–333.

Ernst and Buchan, 1997b. R.E. Ernst and K.L. Buchan , Layered mafic intrusions: a model for their feeder systems and relationship with giant dyke swarms and mantle plumes centres. *South African Journal of Geology* **100** 4 (1997), pp. 319–334.

Glen et al., 1997. J.M.G. Glen, P.R. Renne, S.C. Milner and R.S. Coe , Magma flow inferred from anisotropy of magnetic susceptibility in the coastal Parana–Etendeka igneous province: evidence for rifting before flood volcanism. *Geology* **25** 12 (1997), pp. 1131–1134.

Hargraves et al., 1991. R.B. Hargraves, D. Johnson and C.Y. Chan , Distribution anisotropy: the cause of AMS in igneous rocks?. *Geophysical Research Letters* **18** (1991), pp. 2193–2196.

Hattingh and de Wet, 1996. P.J. Hattingh and J.A.J. de Wet , A palaeomagnetic investigation of the Insizwa intrusives. *South African Journal of Geology* **99.3** (1996), pp. 221–228.

Hawkesworth et al., 1999. C.J. Hawkesworth, S. Kelley, S. Turner, A. Le-Roex and B. Storey , Mantle processes during Gondwana break-up and dispersal. *Journal of African Earth Sciences* **28.1** (1999), pp. 239–261.

Jelínek, 1981. V. Jelínek , Characterization of the magnetic fabrics of rocks. *Tectonophysics* **79** (1981), pp. 63–67.

Knight and Walker, 1988. M.D. Knight and G.P.L. Walker , Magma flow directions in dikes of the Koolau Complex, Oahu, determined from magnetic fabric studies. *Journal of Geophysical Research* **93** B5 (1988), pp. 4301–4319.

Launeau and Robin, accepted for publication. Launeau, P., Robin, P.-Y.F., accepted for publication. Determination of fabric and strain ellipsoids from measured sectional ellipses—Examples. Journal of Structural Geology.

Lightfoot et al., 1984. P.C. Lightfoot, A.J. Naldrett and C.J. Hawkesworth , The geology and geochemistry of the Waterfall Section of the Insizwa Complex with particular reference to the origin of the nickel sulphide deposits. *Economic Geology* **79** (1984), pp. 1857–1879.

Lightfoot et al., 1987. P.C Lightfoot, A.J. Naldrett and C.J. Hawkesworth , Re-evaluation of chemical variation in the Insizwa Complex, Transkei. *Canadian Mineralogist* **25** (1987), pp. 79–90.

Maier et al., 2001. W.D. Maier, J.S. Marsh, S.J. Barnes and D.C. Dodd , The concentrations of the platinum-group elements and gold in the Insizwa lobe, Mount Ayliff Complex, South Africa: implications for Ni–Cu–PGE sulphide exploration in the Karoo Igneous Province. *Economic Geology* (2001) accepted for publication .

Maré and Ousthuizen, 2000. L.P. Maré and B.C. Oosthuizen In: *South African Geophysical AtlasPhysical Properties of South African rocks* **vol. IV**, Council for Geoscience of South Africa (2000) version II, 19 pp.

Maske and Cawthorn, 1986. S. Maske and R.G. Cawthorn , The nickel occurrence in the Insizwa Complex, Transkei. In: C.R. Maske and S. Anhaeusser, Editors, *Mineral Deposits of Southern Africa*, Geological Society of South Africa, Johannesburg (1986), pp. 2149–2158.

McBirney and Nicolas, 1997. A.R. McBirney and A. Nicolas , The Skaergaard Layered Series: Part II. Magmatic flow and dynamic layering. *Journal of Petrology* **38** (1997), pp. 569–580.

Meissner, 1985. R. Meissner , The Continental Crust: A Geophysical Approach. , Academic Press, Orlando (1985) 426 pp. .

Naslund and McBirney, 1996. H.R. Naslund and A.R. McBirney , Mechanisms of formation of igneous layering. In: R.G. Cawthorn, Editor, *Layered Intrusions*, Elsevier, Amsterdam (1996) 531 pp. .

Nicolas, 1992. A. Nicolas , Kinematics in magmatic rocks with special reference to gabbros. *Journal of Petrology* **33.4** (1992), pp. 891–915.

Philpotts et al., 1999. A.R. Philpotts, C.M. Brustman, J. Shi, W.D. Carlson and C. Denison , Plagioclase-chain networks in slowly cooled basaltic magma. *American Mineralogist* **84** (1999), pp. 1819–1829.

Potter and Stephenson, 1988. D.K. Potter and A. Stephenson , Single-domain particles in rocks and magnetic fabric analysis. *Geophysical Research Letter* **15** 10 (1988), pp. 1097–1100.

Pysklywec and Mitrovica, 1999. R.N. Pysklywec and J.X. Mitrovica , The role of subduction-induced subsidence in the evolution of the Karoo basin. *Journal of Geology* **107** (1999), pp. 155–164.

Robin, 2002. P.-Y.F. Robin , Determination of fabric and strain ellipsoids from measured sectional ellipses—Theory. *Journal of Structural Geology* **24** (2002), pp. 531–544.

Rochette, 1987. P. Rochette , Magnetic susceptibility of the rock matrix related to magnetic fabric studies. *Journal of Structural Geology* **9** (1987), pp. 1015–1020.

Rochette et al., 1999. P. Rochette, C. Aubourg and M. Perrin , Is this magnetic fabric normal ? A review and case studies in volcanic formations. *Tectonophysics* **307** (1999), pp. 219–234.

Sack et al., 1980. R.O. Sack, I.S.E. Carmichael, M. Rivers and M.S. Ghiorso , Ferric–ferrous equilibria in natural silicate liquids at 1 bar. *Contribution to Mineralogy and Petrology* **75** (1980), pp. 369–376.

Sander, 1993. Sander, B.K., 1993. Aspects of the geology and sulphide ore potential of the Mount Ayliff Intrusion, Transkei. PhD, University of the Witwatersrand, South Africa, 340 pp.

Sander and Cawthorn, 1996. B.K. Sander and R.G. Cawthorn , 2.5-D gravity model of the Ni–Cu–PGM mineralized Mount Ayliff Intrusion (Insizwa Complex), South Africa. *Journal of Applied Geophysics* **35** (1996), pp. 27–43.

Scholtz, 1937. D.L. Scholtz , The magmatic nickeliferous ore deposits of East Griqualand and Pondoland. *Transaction of Geological Society of South Africa* **39** (1937), pp. 81–210.

Smith, 1990. R.M.H. Smith , A review of stratigraphy and sedimentary environments of the Karoo basin of South Africa. *Journal of African Earth Sciences* **10** (1990), pp. 117–137.

Stephenson, 1994. A. Stephenson , Distribution anisotropy: two simple models for magnetic lineation and foliation. *Physics of the Earth and Planetary Interiors* **82** (1994), pp. 49–53.

Syono, 1960. Y. Syono , Magnetic susceptibility of some rock forming silicate minerals such as amphiboles, biotites, cordierites and garnets. *Journal of Geomagnetism and Geoelectricity* **11** (1960), pp. 85–93.

Tarling and Hrouda, 1993. D.H. Tarling and F. Hrouda , The Magnetic Anisotropy of Rocks. , Chapman & Hall, London (1993) 217 pp. .

Tauxe, 1998. L. Tauxe , Paleomagnetic Principles and Practice. , Kluwer Academic Publishing, Dordrecht (1998) 299 pp. .

Taylor, 1988. H.P. Taylor, Jr. , Oxygen, hydrogen and strontium isotopes constraints on the origin of granites. *Transactions of the Royal Society of Edinburgh, Earth Sciences* **79** (1988), pp. 317–338.

Turner, 1999. B.R. Turner , Tectonostratigraphic development of the Upper Karoo foreland basin: orogenic unloading versus thermally-induced Gondwana rifting. *Journal of African Earth Sciences* **28** (1999), pp. 215–238.

White and McKenzie, 1989. R.S. White and D.P. McKenzie , Magmatism at rift zones: the generation of volcanic continental margins and flood basalts. *Journal of Geophysical Research* **94** (1989), pp. 7685–7729.

Wylie et al., 1999. J.J. Wylie, K.R. Helfrich, B. Dade, J.R. Lister and J.F. Salzig , Flow localization in fissure eruptions. *Bulletin of Volcanology* **60** (1999), pp. 432–440.